Tectonophysics 796 (2020) 228629

Contents lists available at ScienceDirect

Tectonophysics

journal homepage: www.elsevier.com/locate/tecto

# Seismic structure and tectonics of the continental wedge overlying the source region of the Iquique Mw8.1 2014 earthquake

Gabino Reginato [a,*], Emilio Vera [a], Eduardo Contreras-Reyes [a], Anne M. Tréhu [b], Andrei Maksymowicz [a], Juan Pablo Bello-González [c,d], Felipe González [a]

[a] Departamento de Geofísica, Facultad de Ciencias Físicas y Matemáticas, Universidad de Chile, Santiago, Chile
[b] College of Earth, Ocean, and Atmospheric Sciences, Oregon State University, Corvallis, OR, USA
[c] Grupo Minero Las Cenizas, Taltal, Chile
[d] Departamento de Geología, Facultad de Ciencias Físicas y Matemáticas, Universidad de Chile, Santiago, Chile

ARTICLE INFO

*Keywords:*
Iquique
Chile
Earthquake
Subduction
Continental wedge
Seismic reflection

ABSTRACT

On April 1, 2014, a large earthquake (Mw = 8.1) ruptured the central part of a historic seismic gap in northern Chile. In order to study the relationship between the co-seismic rupture characteristics and the crustal structure of the subduction zone, we processed a trench-perpendicular seismic reflection profile acquired across the zone of maximum slip and generated a P-wave velocity model. The results show a frontal prism in the continental wedge characterized by low velocities that increase rapidly towards the shore and acted as a barrier for trench-ward propagation of aftershocks. Landward, a transition zone with increasing upper crust velocity (4–5 km/s) concentrates most of the aftershocks. In addition, a trench-ward dipping set of fault zones is observed along the continental wedge associated to the Iquique forearc basin formation (1.5 km thick at the depocenter on this profile). We identify three stratigraphic units within the basin. A landward tilt and thickness increase is detected in each stratigraphic unit, along with growth strata and domino structures, suggesting landward migration of *syn*-extensional deformation in response to basal subduction erosion. By extrapolating our results to the plate boundary and based on published focal mechanisms of intra-crustal seismicity, we find a strong spatial correlation between the Iquique basin and the highest slip area for the 2014 earthquake, suggesting long-term extensional deformation due to coseismic tensional stresses.

## 1. Introduction

Prior to the April 1, 2014, Mw 8.1 Iquique earthquake, the segment of the Nazca-South America subduction margin between 19°S and 21°S had not experienced a large earthquake since the historic 1877 Mw 8.8 megathrust earthquake (Comte and Pardo, 1991). The main shock ruptured a zone approximately 100 km-long parallel to the trench axis from 19°30′S to 20°30′S and covered approximately 1/3 of the historic seismic gap (Ruiz et al., 2014; Kato and Nakagawa, 2014; Lay et al., 2014). According to the slip models (e.g. Ruiz et al., 2014; Lay et al., 2014; Schurr et al., 2014; Duputel et al., 2015), the earthquake rupture did not extend up-dip to the trench (Fig. 1), with an up-dip limit ~20 km deep and 70 km landward of the trench.

The Iquique earthquake is characterized by: (1) an extended and well-characterized sequence of seismic events in the months and weeks prior to the main shock, and (2) a high correlation between this sequence and negative anomalies in the earth's gravity field (Maksymowicz et al., 2018; Ruiz et al., 2014; Álvarez et al., 2018). It has been proposed that these latitudinal variations in gravity, due to latitudinal variations of mean density in the continental wedge, result in a seismic segmentation of the Northern Chile subduction margin, where mechanically differentiated segments can be activated in a complex sequence of large events. These correlations between gravity and slip distribution have been originally observed by Song and Simons (2003) and Wells et al. (2003), and supported by more recent studies (Álvarez et al., 2014; Álvarez et al., 2019; Bassett and Watts, 2015; Bassett et al., 2016; Li and Liu, 2017; Spagnotto et al., 2018).

High-resolution seismic reflection data have been interpreted to characterize the structural and stratigraphic framework along the Andean forearc (e.g. Contardo et al., 2008; Geersen et al., 2018; Becerra et al., 2013, 2017; Maksymowicz et al., 2018; Tréhu et al., 2020).

For example, Becerra et al. (2017) reveals several tectonic phases

* Corresponding author.
*E-mail address:* gab.reginato01@gmail.com (G. Reginato).

https://doi.org/10.1016/j.tecto.2020.228629
Received 12 March 2020; Received in revised form 12 September 2020; Accepted 12 September 2020
Available online 15 October 2020

during Cenozoic times. If geochronological data of stratigraphic units are lacking (as in our case), the shield kinematic evolution can be relatively constrained, without absolute temporal reference. Here, we use high quality seismic data acquired during the PICTURES (Pisagua Iquique Crustal Tomography to Understand the Region of the Earthquake Source) project (Fig. 1) to examine the seismic structure of the marine forearc of the northern Chilean margin and correlate it with the earthquake slip and aftershock distribution. The seismic data is also used to interpret the tectonic development of the offshore forearc, providing valuable information about long term tectonic processes.

## 2. Seismotectonic and geological setting

In the study area, the Nazca plate subducts beneath the continental South American plate at a current rate of 72 mm/year (DeMets et al., 2010, Fig. 2). Because of this subduction process, the oceanic Nazca plate flexes in the forearc region, resulting in high tensional stresses and the formation of a pronounced outer rise and a horst and graben system with up to 500 m of vertical displacement (Ranero et al., 2006; Contreras-Reyes et al., 2012; Geersen et al., 2018). Due to the arid climate and the consequent low sedimentation rate to the trench, these bathymetric highs and lows are not filled, resulting in an extremely rough subducting surface (Contreras-Reyes, 2018). One of the effects of this roughness is the favoring of subduction erosion (Von Huene et al., 1985; Von Huene et al., 1999) and landward migration of the trench accompanied by eastward migration of the magmatic arc by ~200 km since at least the Jurassic era (eg. Rutland, 1971; Schellart, 2017). The subduction erosion also causes tensional stresses in the continental wedge, generating normal faults along the continental slope, trenchward steepening of the slope, and terrace formation near the coast (Armijo and Thiele, 1990; Delouis et al., 1998; Von Huene and Ranero, 2003; Contreras-Reyes, 2018).

Gravimetric and seismic tomography models (Contreras-Reyes et al., 2012; Maksymowicz et al., 2018) in the study area show the presence of a ~ 10 km wide low density zone associated with a frontal prism formed by eroded material from the upper plate. Density and P-wave velocity increase rapidly landward due to compaction of the frontal prism and decrease in fracturing (Sallares and Ranero, 2005: Contreras-Reyes et al., 2012; Contreras-Reyes, 2018). The continental crust is also characterized by the presence of a low density and low velocity zone in its trenchward part, which is interpreted as a consequence of high fracturing associated with subduction erosion (e.g., Maksymowicz et al., 2018). Relocation of aftershocks of the Iquique earthquake (León-Ríos et al., 2016) show that the aftershocks do not occur near the trench (Fig. 2. This low velocity zone is expected to be associated with stable slip and aseismic deformation. It has also been proposed in accretionary margins (Wang and Hu, 2006) that the most seaward part of an accretionary prism (the outer wedge) overlies the up-dip velocity-strengthening part of the subduction fault, and that the less deformed inner wedge overlies the velocity-weakening part (the seismogenic zone).

Onshore, the forearc geology in this central Andean region consists of four morphostructural units. From west to east these are the Coastal Cordillera, Central Depression, Forearc Precordillera, and Western Cordillera (Fig. 1, e.g. Charrier et al., 2013). Mesoproterozoic zircon ages have been found in rocks exposed in the forearc Precordillera near Quebrada Choja, and Belén, 225 km SW and 160 km NE, respectively, from the eastern end of MC06 (Loewy et al., 2004). On the other hand, dating of detrital zircons analysis presented by Bahlburg et al. (2009) for

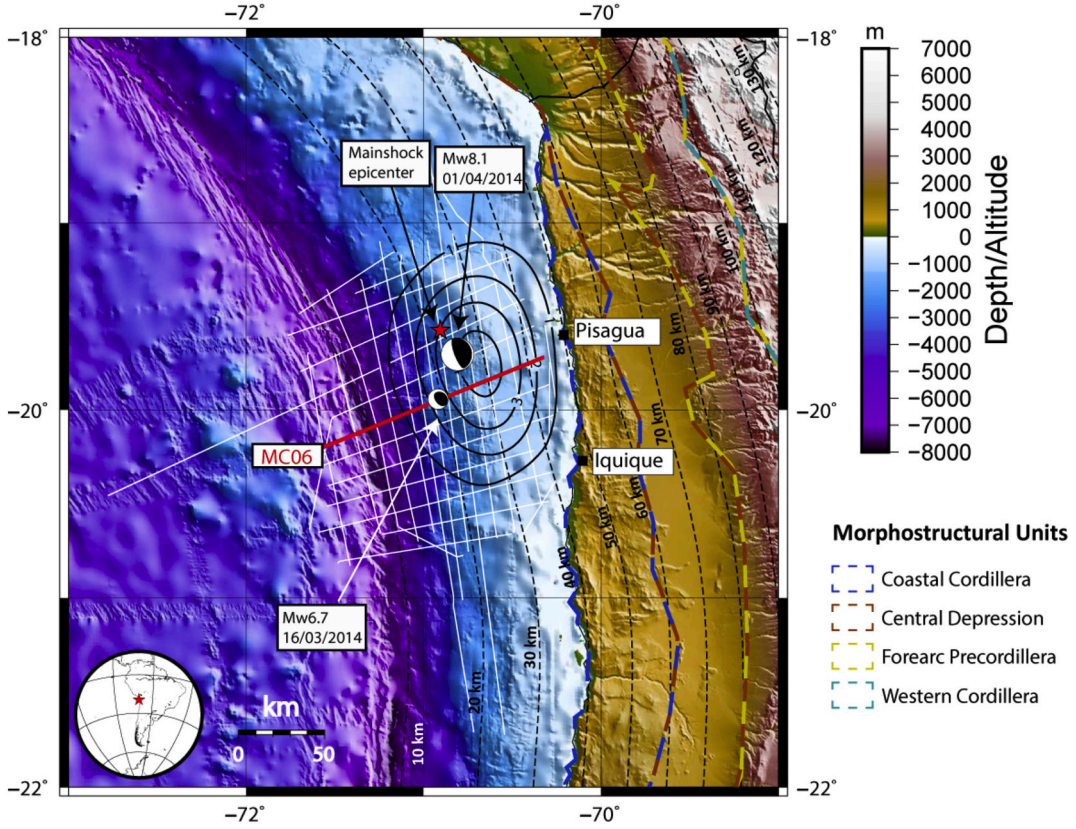


**Fig. 1.** The PICTURES seismic profiles are shown as white lines. The MC06 line used for this study is shown in red. The red star corresponds to the epicenter of the Iquique earthquake. Solid black lines are contour lines of the slip during the 2014 Iquique earthquake (Schurr et al., 2014). MC06 (thick red line) crosses the area of highest coseismic slip during the mainshock as well as the source region of the March 16 (Mw = 6.7) foreshock. Black dashed lines correspond to SLAB 1.0 (Hayes et al., 2012) model for the subduction interface (at 10 km interval). Bathymetry from ETOPO1. (For interpretation of the references to colour in this figure legend, the reader is referred to the web version of this article.)

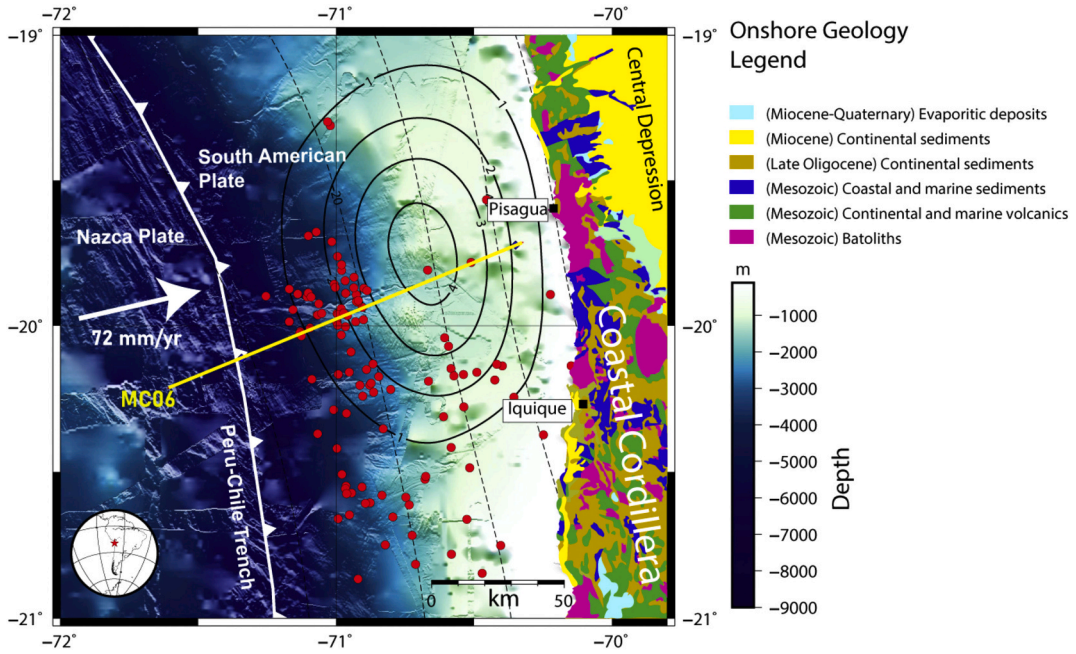


**Fig. 2.** The Iquique earthquake slip distribution (black solid lines) and relocated aftershocks (León-Ríos et al., 2016) in red dots. The yellow line represents line MC06 of the PICTURES project. White arrow represents the convergence velocity vector between Nazca and South America (fixed) plates from DeMets et al. (2010), Bathymetry from ETOPO1. Onshore geology units were obtained from SERNAGEOMIN (2003). (For interpretation of the references to colour in this figure legend, the reader is referred to the web version of this article.)

an outcrop about 200 km south of the M06 profile in the Coastal Cordillera imply a possible Paleoproterozoic crustal basement as far north as 20–21°S. During the Jurassic and Early Cretaceous a subduction-related magmatic arc system developed along the present-day Coastal Cordillera (Oliveros et al., 2007). The resulting Jurassic volcanic and sedimentary units crop out as homoclinal sequences that can reach thicknesses of 7000 to 10,000 m (Buchelt and Tellez, 1988). Geochemical analyses indicate that western South American margin in the latitude of this study underwent tectonic stretching and lithospheric thinning during Late Permian to Late Jurassic (Sempere et al., 2002; Mamani et al., 2010; Oliveros et al., 2020).

The Western Cordillera has provided sediment in-filling the Central Depression and paleo-basins within the Coastal Cordillera since at least the Late Oligocene under an arid to semi-arid regime (Evenstar et al., 2017). A major uplift episode at ~23 Ma preserved the Coastal Tarapacá Surface as a relict paleosurface within the Coastal Cordillera, shown as Late Oligocene continental sediments in Fig. 2 (Dunai et al., 2005). This ~23 Ma Uplift of the Coastal Cordillera resulted in a substantial barrier to the westward flowing sedimentary systems, retaining Miocene and younger sediments within the Central Depression (Miocene continental sediments in Fig. 2). However, this blockage of sediment discharge behind the Coastal Cordillera could have cause starvation of sediment accumulation in the trench (Delouis et al., 1998; Hartley et al., 2000; Wörner et al., 2002; Dunai et al., 2005).

Uplift rates are poorly constrained but generally believed to have been between 0.04 mm/yr to 0.07 mm/yr (Delouis et al., 1998; Dunai et al., 2005). Furthermore, Melnick (2016) estimated long term uplift rates of 0.13 ± 0.04 mm per year along the Coastal Cordillera relief of central Andes during the Quaternary using morphometry and a landscape evolution model of coastal erosion. On the other hand, the characteristic coastal escarpment of north Chile has been interpreted as a relict of long term uplift process and has been maintained by the extremely small denudation rate of the Atacama Desert (Dunai et al., 2005; Carrizo et al., 2008; Evenstar et al., 2009; Cosentino and Jordan, 2017).

## 3. Seismic data and processing

### 3.1. Seismic data acquisition

In order to map the subsurface in the study area, a network of OBS (Ocean Bottom Seismometers) and land seismometers was deployed to record seismic signals generated by the R/V *Marcus Langseth* during cruise MGL1610 by an array of 40 airguns of 6600 cubic inches of total source volume. The shots were also recorded on *Langseth*'s 8 km-long, 648-channel streamer in 16 s long records with 2 ms sampling interval. These shots were fired in a grid consisting of 32 seismic profiles that cover the whole rupture zone. Here, we present line MC06 (red line in Fig. 2) that was processed to obtain a seismic reflection profile and a 2D P-wave velocity model from the streamer data. This line runs perpendicular to the trench axis, crossing the area of highest coseismic slip and directly over the March 16 (Mw = 6.7) foreshock. The shots in this line were fired every 125 m, with a spacing of 12.5 m between each geophone with the first geophone 220 m away from the source. This geometry results in common mid points (CMP) every 6.25 m, with 32 or 33 seismic traces for each CMP.

### 3.2. Data processing

#### 3.2.1. Seismic reflection profile

In order to obtain a time-migrated seismic section (Fig. 3), a standard processing sequence was carried out over the multichannel data of the MC06 line using Seismic Unix routines. These steps include CMP geometry sorting; application of a predictive deconvolution filter; semblance velocity analysis over 50 common mid points along the line; normal move out correction and muting; stacking and post-stack migration using water velocity (1500 m/s). To reduce refraction arrivals at larger offsets and enhance the observed reflections, only the first 324 channels of the streamer were used for the reflection image (maximum offset of 4 km). Raw records were resampled from 2 ms to 4 ms to reduce computation time.

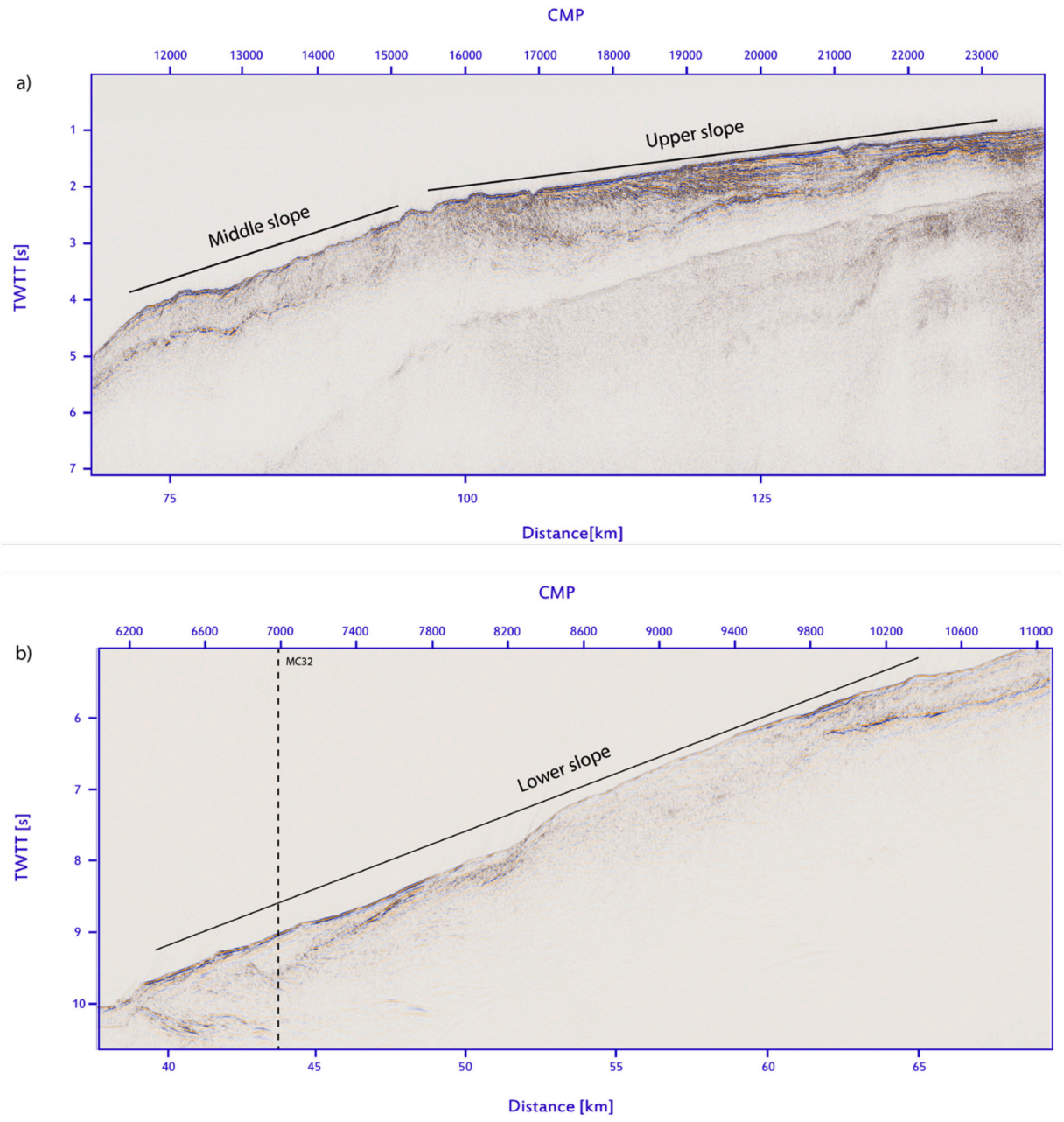


**Fig. 3.** Seismic line MC06 after Normal Move Out (NMO), Muting, Stacking and a Post-Stack Time Migration with water velocity. (a) Middle and Upper slope, (b) Lower slope.

### 3.2.2. *P-wave velocity model*

To construct the 2D P-Wave velocity model, 20 adjacent CMPs were resorted to form a new CMP ("supergather') with 648 traces spaced 6.25 m apart and representing source-receiver offsets of 220-8300 m. Arrival times of reflections and refractions were then forward-modeled using a 1D velocity model representative of the center of this 125 m wide bin formed by 20 CMPs to generate a Vp model with four or five constant velocity or constant gradient layers. This grouping was made every 256 CMPs, which means there is one 1D velocity model every 1600 m (Fig. 4). Intermediate velocity models were then constructed by horizontal linear interpolation.

### 3.2.3. *Time (TWTT) to depth conversion*

The time it takes for a P-Wave to go back and forth to a reflector located a depth dz., is dt = 2* dz./v, so if we know the velocity and reflection time (TWTT), we can now calculate the depth of the reflector. With a velocity model for each CMP, we can transform the Two Way Travel Time (TWTT) to depth using the corresponding 1-D velocity model:

$$Z_1 = \frac{\mathrm{dt}}{2} v(\mathrm{z}=0) \tag{1}$$

$$Z_n = \mathrm{Z}_{n-1} + \frac{\mathrm{dt}}{2} v(Z_{n-1}) \tag{2}$$

here $Z_1$ corresponds to the physical location in depth of a reflection registered at time $t = dt^* Z_n$ corresponds to the depth of a reflection occurring a $t = n^*dt$. The new sampling in depth is dz. $= dt/2 \ ^*V_{min}$, with $dt = 4$ ms (time sampling of the original trace) and $V_{min} = 1.5$ km/s. This results in a depth sampling interval of $dz = 3$ m.

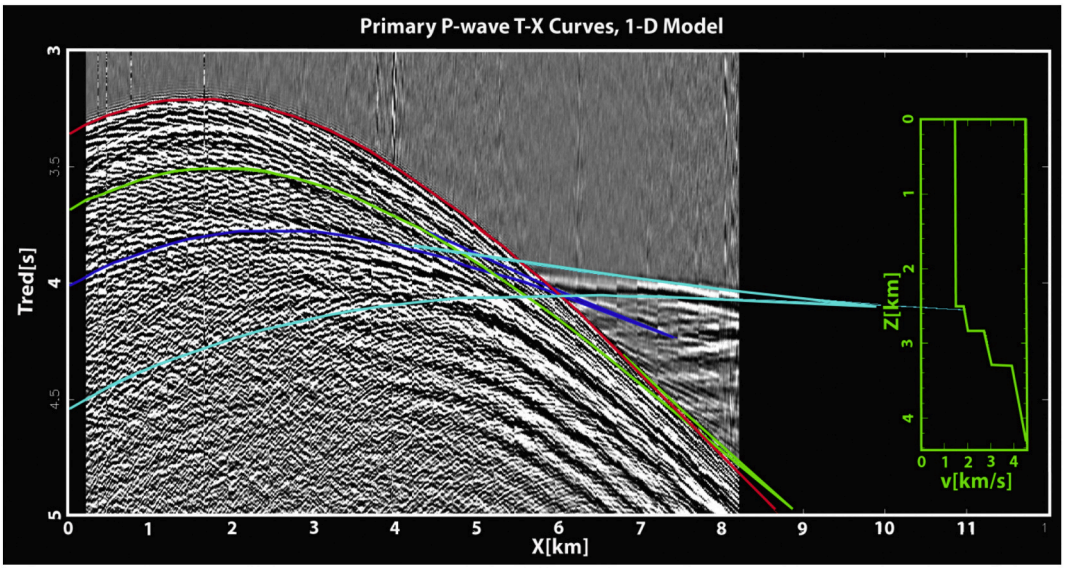


**Fig. 4.** Example of a supergather with predicted arrival times of reflections and refractions in different layers. The velocity model used is shown on the right. CMPs 13,568–13,587 (d = 84.8 km). A reduction velocity of 5 km/s is used.

## 4. Results and interpretation

The reflection profile converted from TWTT to depth is shown in Fig. 5 overlain on the velocity model. To transform the reflection profile below the known velocity, a constant velocity of 6 km/s was used (not shown in the profile). This velocity of 6 km/s is used as it is a reasonable velocity for the continental crust. From what is seen in the reflection profile and velocity model, the sediment thickness in the trench, is very thin (<1 km), similar to what is found in previous works (e.g. Contreras-Reyes et al., 2015; Maksymowicz et al., 2018). Landward, the continental wedge is characterized by three differentiated sections. The first section (Lower slope), from the trench to ~75 km (along the profile), has a seafloor slope of approximately 6.5 degrees. This section is characterized by a very low-velocity (2–3 km/s) frontal zone, located between kilometer 35 and 45, and probably consists of eroded sediments from the slope. East of km 45, it presents higher velocities (3–4 km/s), which probably indicate highly fractured upper crust. The second section (middle slope), between km 75 and 105, has a seafloor slope of 3°. This zone, which includes the western limit of the Iquique Basin at ~km 95, is characterized by several seaward dipping scarps, indicating extensive normal faulting in the continental basement (Fig. 5). The third section (upper slope, east of km 105), with seafloor slope of approximately 1.5 degrees, has extensive normal faulting in the continental basement. Sediments deposited over this faulted surface form the Iquique Basin, which shows extensive normal faulting extending to the seafloor.

As mentioned previously, the lower slope (outer wedge) is characterized by a frontal low velocity zone (Figs. 5 and 6), with values between 2 km/s and 3 km/s. This zone is interpreted as a deformed region associated to the frontal prism (Contreras-Reyes et al., 2012; Maksymowicz et al., 2018), with thrust faults from a basal detachment surface (decollement) that generate antiformal stack geometry. The landward bound of this prism lies approximately at km 45 of the seismic profile (Fig. 6). Here, the average initial subduction angle is about 4°.

Landward of the imaged frontal prism (Figs. 5 and 6), still in the lower slope, the velocity model shows a higher velocity zone (3–4.5 km/s) associated to a high fractured continental crust between 45 and 55 km (Contreras-Reyes et al., 2012; Maksymowicz et al., 2018). Below the lower slope, the MCS profile reveals some normal faults reaching the seafloor, which coincide with horizontal $V_p$ changes in the velocity model. Some trenchward dipping normal scarps are identified on the

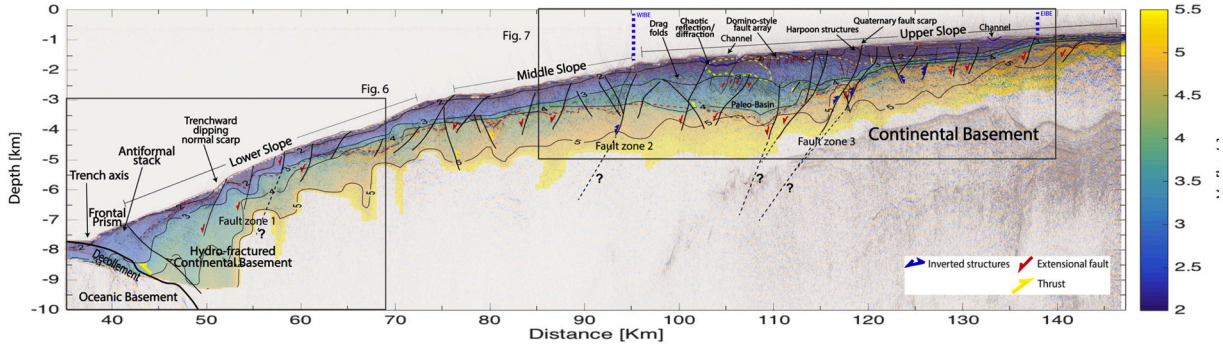


**Fig. 5.** Combined interpreted seismic profile and 2D velocity model along seismic line MC06. Segmented green lines represent main unconformities that define the tectono-stratigraphy unit boundaries, continuous wide and thin black lines depict principal and secondary faults respectively, interpreted from seismic profile, and segmented black lines show the inferred projection of main structures in the acoustic basement, blue lines depict the interpreted paleo-channel filled, yellow segmented line bound the chaotic reflection zone. (For interpretation of the references to colour in this figure legend, the reader is referred to the web version of this article.)

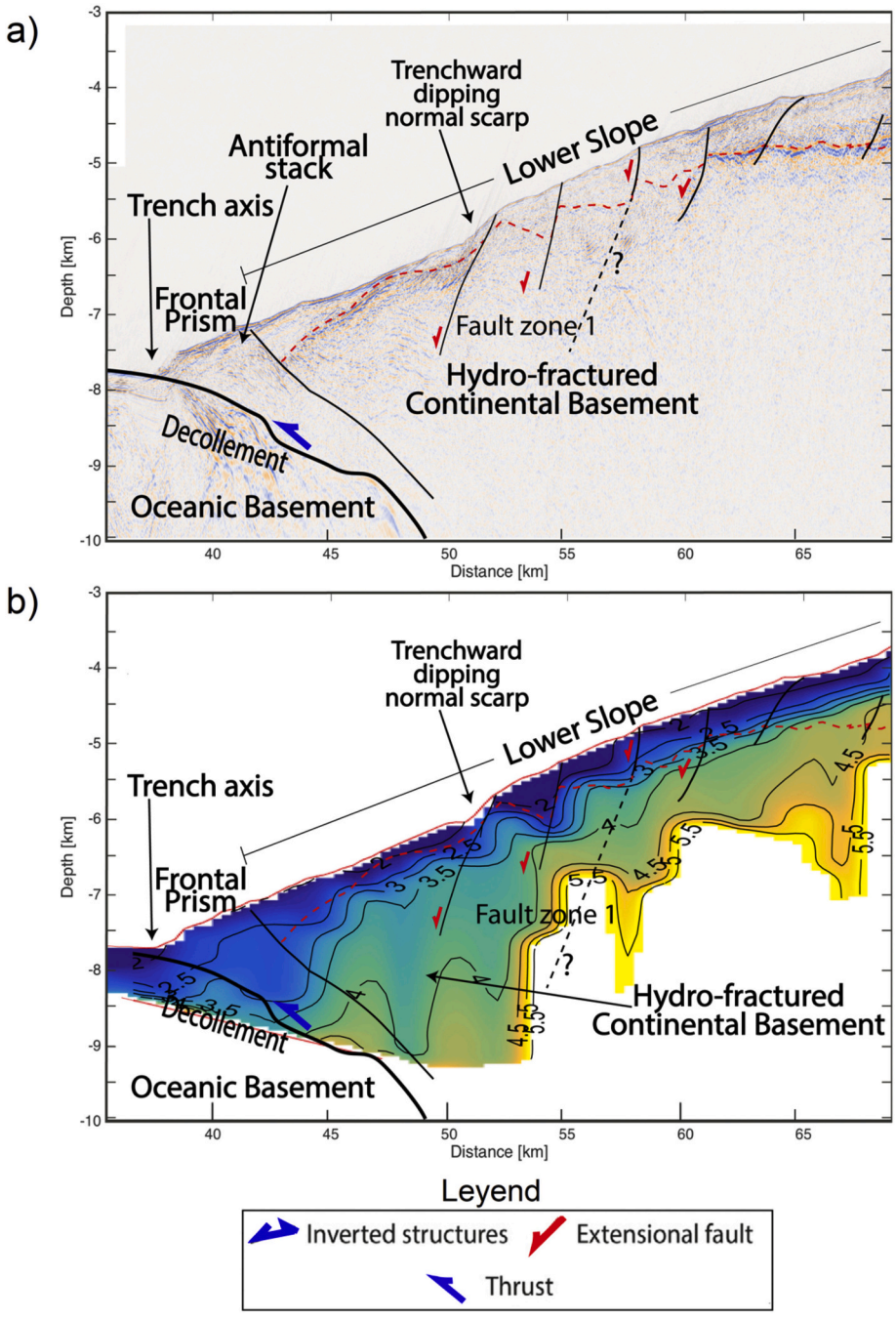


**Fig. 6.** (a) Seismic profile and (b) Vp section and interpreted seismic profile of the frontal prism and fractured continental crust zone. Black dashed lines represent the landward limit of fractured continental crust zone. In black solid lines, we show principal faults, colored arrows represent fault kinematics (thrust: blue, normal: red). Dotted red line highlights the reflector R (see main text for details). (For interpretation of the references to colour in this figure legend, the reader is referred to the web version of this article.)

seafloor and interpreted as normal faults extending to greater depth. Sharp differences in $V_p$ velocities and interpreted stratigraphic unconformities are used to delineate the top of continental basement (Fig. 6). A prominent reflector (R) semi-parallel to the seafloor appears (Fig. 6) overlying the highly deformed and fractured crust mentioned above. Above this reflector, we find low velocity sediments, which seem to have low deformation and sedimentation approximately parallel to the reflector R and the seafloor. These sediments are probably eroded from the continental slope and flow towards the trench and frontal prism. Landward (between kilometers 52 and 60), we find a section of the seismic profile where is difficult to appreciate the sediment/crust transition, and an upper crust with less internal reflectors when compared to the hydro-fractured frontal zone. Between kilometers 60 and 70 the transition between the sediments and continental crust becomes clear, suggesting a sharper change in P-wave velocity than in the previous section, as seen in the Vp model.

The middle and upper slopes (inner wedge) are characterized by extensive normal faulting in the continental basement, which produces a 1–1.5 km deep depression in the continental basement called the Iquique Basin. This basin is covered by different sediment units (Figs. 5 and 7).

At the trenchward side and middle section of the forearc section, the seismic profile shows a lower stratigraphic unit (SU) 1 of 1 km-thick. This unit shows a velocity of ~3.5 km/s; here interpreted as old and very well compacted sediments. Inside this layer, the pattern of sedimentation is not well distinguishable. The intermediate SU2, characterized by a thickness of 1 km and $V_p$ ranging between 2.0 and 3.0 km/s, is not recognizable in the western side of the basin becoming clearer in the

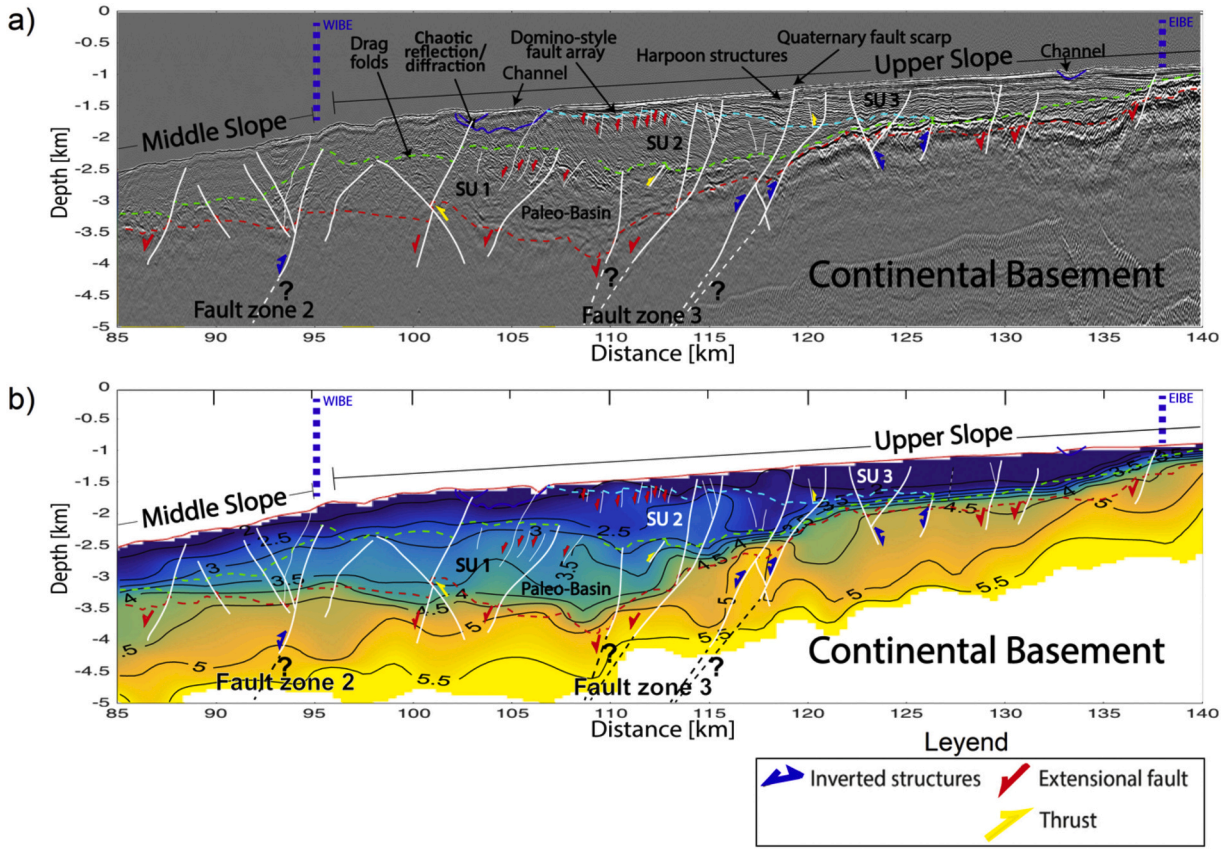


**Fig. 7.** (a) Combined seismic profile and (b) velocity model of the Iquique basin. White lines depict where major faults were interpreted, narrow white lines represent secondary faults. Dashed red/green/light blue lines mark the transitions between different stratigraphic units (SU 1, 2 and 3), based on velocity and distinguishable unconformities. Red arrows represent fault kinematics of normal, yellow arrows thrust faults, blue double vergence arrows shows kinematics of inverted faults. (For interpretation of the references to colour in this figure legend, the reader is referred to the web version of this article.)

center. A younger and thinner SU 3 layer of low velocity sediments (~2 km/s) covers the whole landward side of the basin, thinning towards the center of the basin until disappearing. On the east side, growth strata configuration and normal faulting can be recognized, suggesting an active extensional deformation process.

All stratigraphic units show an increase in thickness eastward until a main trenchward dipping normal structure cuts them. In the case of the fault that marks the thickest part of SU 2, the normal kinematics has been inverted, as indicated by a harpoon anticline located in SU 3 (Fig. 7). This is a classic geometry for tectonic inversion. In addition, we

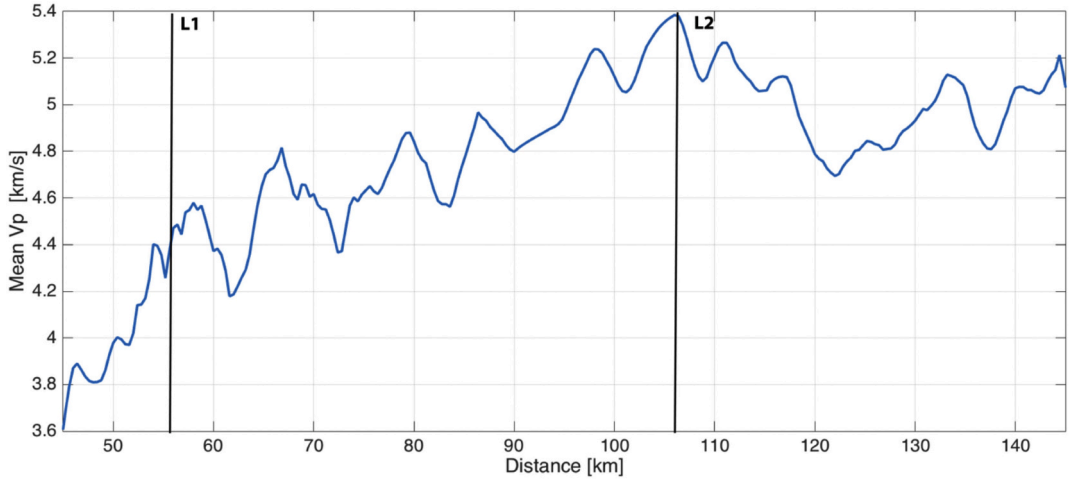


**Fig. 8.** Mean velocity of the first km continental crust. Red dashed lines represent the trend of this velocity and black lines mark where this trend changes (L1 and L2). The velocity trend landward of km 105 is taken considering only the beginning and end velocity of this section, as a straight line cannot be fitted in the data. (For interpretation of the references to colour in this figure legend, the reader is referred to the web version of this article.)

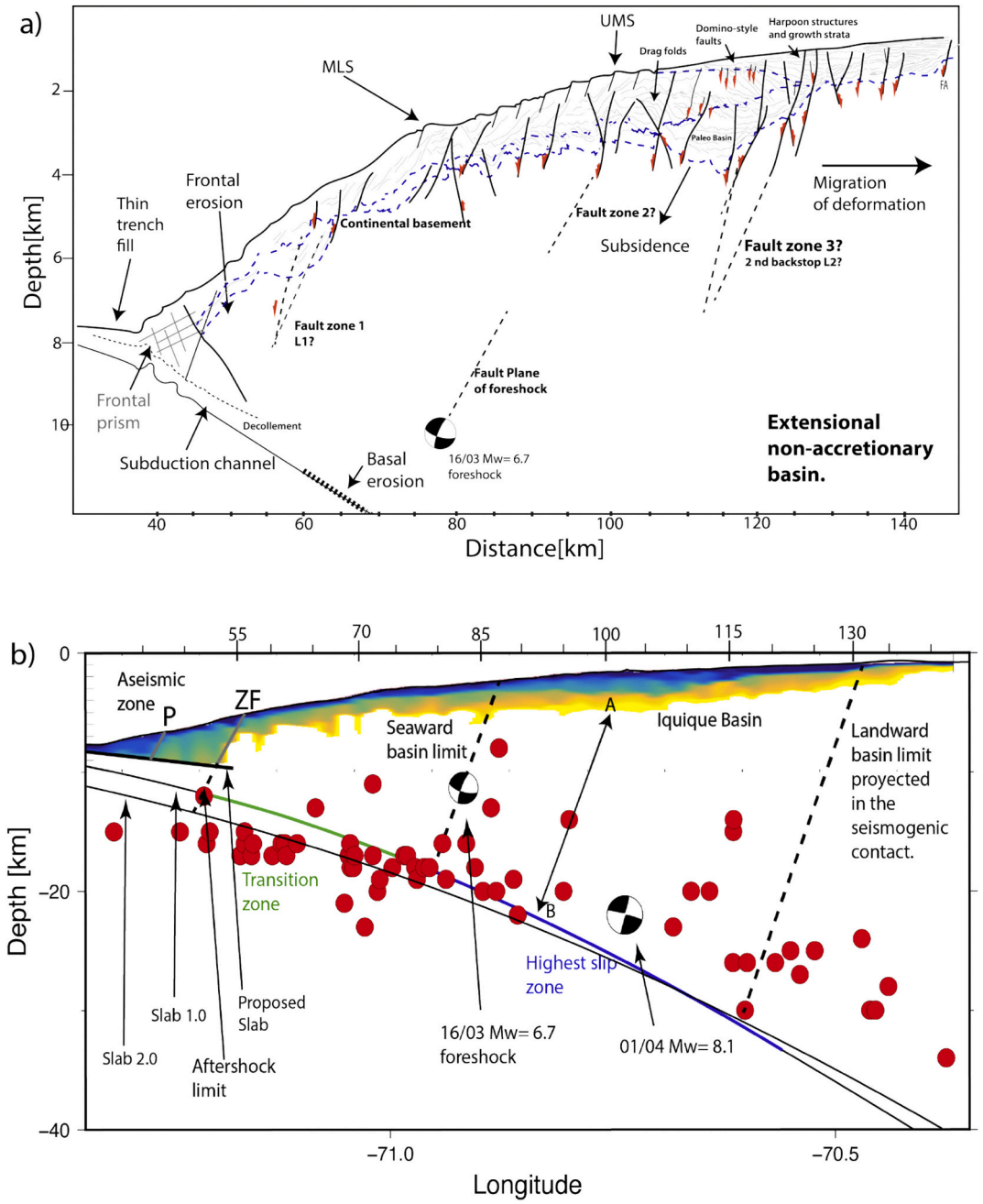


**Fig. 9.** (a) Structural model along seismic profile MC06. A sediment-depleted trench and a subduction channel. A frontal prism (between the trench axis and P) and a highly fractured continental crust (between P and ZF). Seaward dipping scarps in the ocean floor and normal faulting in the continental basement, the Upper-Middle slope transition (UMS) and the Middle-Lower slope transition (MLS). Also is shown the focal mechanism of the 16/03 $M_w$ 6.7 reverse foreshock and the preferred rupture plane. The arrow between A and B represents how these points are spatially correlated. This arrow has the same dip as the main faults, such as the rupture plane of the $M_w$ 6.7 foreshock. (b) Velocity model along seismic line MC06 with relocated aftershocks (León-Ríos et al., 2016) along the profile. Slab 1.0 from Hayes et al. (2012) is shown divided in three zones. Black: Aseismic zone (no aftershocks), Green: Aftershock zone, Blue: Main rupture zone. (For interpretation of the references to colour in this figure legend, the reader is referred to the web version of this article.)

note that the depocenter of the younger stratigraphic units is located eastward in the Iquique Basin. The faults observed at the eastern side of the depocenter likely controlled each SU in a synextentional tectonic regime. In the case of SU 2, the now inverted eastern branch of fault zone 3 has driven growth strata also in SU 3, which tilted landward, associated to *syn*-extensional deposition. This landward tilt suggests that basal erosion dominated over frontal erosion and that the depocenter and deformation should migrate landward (Noda, 2016). In SU 1 and 2, between fault zones 2 and 3, many normal faults are clearly visible, showing a domino extensional array, suggesting that these stratigraphic units were also affected by syn-extensional strengths. The SU 1 of well compacted sediments is then interpreted as the deposition of sediments in a paleo-basin (western/seaward side) and the upper layers are the deposition of younger sediments in the eastern/landward side of the basin, where main structures are currently inverted (Fig. 7). This configuration, with older sediments in the trenchward side agrees with the landward migration of the depocenter.

## 5. Discussion

Based on the velocity model, we calculated the mean velocity of the first km of the upper continental crust along the profile between the top of the basement and the lowest resolved velocity (Fig. 8). We found that in the first 20 km, between the trench and L1, the velocity increases rapidly. In the next 50 km, between L1 and L2, the mean velocity continues increasing but at a lower rate. Landward of L2 velocity remains almost constant when comparing the beginning and the end velocity of the section, but presents a decrease of mean velocity in the middle. L1 coincides with the fault zone 1 reinforcing the hypothesis of a highly fractured continental crust near the trench. L2 coincides with the depocenter of the Iquique basin and the presence of growth strata in SU 2 and 3.

Most of the aftershocks of the Iquique earthquake (Figs. 2 and 9) occured between km 55 and 95 of line MC06 (between ~10 and 20 km deep), which is a transition region (Fig. 9) between the highest coseismic slip area (Fig. 10) and an aseismic zone (Soto et al., 2019). The western edge (L1) corresponds to an abrupt change in trend of seismic velocities. This trenchward velocity contrast (L1) is likely related to the transition from a highly fractured continental crust (Vp < 4.5 km/s) to a less fractured one. As a highly fractured unit, it is probably highly hydrated reducing the frictional coefficient at the seismogenic contact and therefore reducing the capacity to accumulate stress, resulting in an aseismic contact. Moreover, the rheology associated to highly fractured material in the outer wedge favored the generation of a subduction channel that smooths the interplate contact and facilitates aseismic slip (Noda, 2016). It has been proposed that in non-accretionary margins such as this, most of the outer wedge lies above the velocity strengthening zone preventing stress accumulation, coseismic slip and high extensional deformation in the lower slope (Wang and Hu, 2006; Geersen et al., 2018).

The general deformation style of the landward limit of the outer wedge (fault zone 1) and the main structures that control the long-term deformation of the Iquique Basin (as fault zones 2 and 3) shows a clear westward dipping direction (Figs. 5, 6 and 7). Then, in order to analyze a possible link between observed deformation and seismotectonics of the interplate boundary, we correlate the oblique projections at depth of the main structures with seismicity (Fig. 9b). This interpretative strategy is implemented considering that stresses occurring in the interplate contact have a great influence in the direction of the main upper plate structures (or at least in a similar direction). This is supported by the focal mechanism of the main forearc intraplate seismicity (eg. Ruiz et al., 2019). It is important to highlight that the largest foreshock ($M_w$ = 6.7) of March 16 (Fig. 9) has a reverse fault mechanism within the continental plate (at about 10 km deep), with a rupture plane that extended from 3 to 17 km depth (Ruiz et al., 2014; Ruiz et al., 2019). The fault plane dip (~70°) coincides approximately with the orientation of the normal faults seen in the shallow part of our our seismic image (Figs. 5 and 7). This presumably large fault (fault plane) outcrops at the middle-upper slope transition as fault zone 2 (Fig. 9). The coincidence of apparent normal faults with intraplate thrust earthquakes has been explained as result from coseismic extension followed by interseismic compression (Delouis et al., 1998). This behavior has been observed in other zones by Delouis et al. (1998) off north Chile at ~23°S, Farías et al. (2011) for the Pichilemu faults off Maule in central Chile at ~34°S and Contreras-Reyes et al. (2015) in Valparaiso Forearc Basin (31–33°S).

Analyzing the aftershock seismicity, the landward limit of the high density aftershock zone (Soto et al., 2019) spatially correlates approximately with the western limit of the Iquique Basin, which is also the updip limit of the highest slip zone (Fig. 9). According to Geersen et al. (2018), this outer wedge zone undergoes compression after coseismic slip, being the aftershocks at the base of the inner wedge, a response to this compressional stress. Landward, the inner wedge lies above the velocity weakening part of the interplate contact (Wang and Hu, 2006). This behavior leads to interseismic stress accumulation due to high

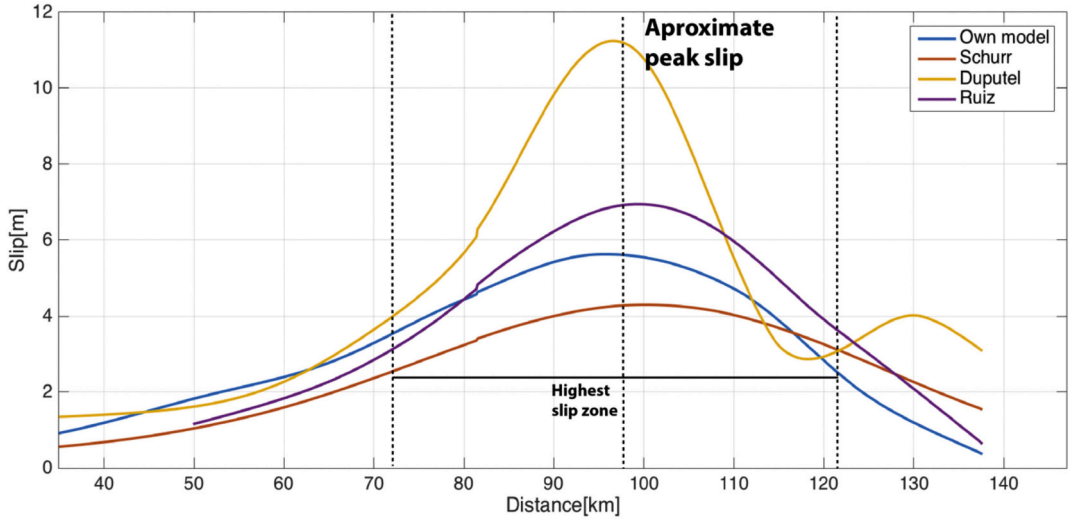


**Fig. 10.** Coseismic slip distribution along profile MC06 of Ruiz et al. (2014), Schurr et al. (2014), Duputel et al. (2015) and a slip model calculated for this paper (see Appendix 1), of the Iquique earthquake.

coupling followed by coseismic slip that generates extensional stresses that produces normal faulting along the inner wedge (e.g., Geersen et al., 2018).

The landward velocity contrast (L2) corresponds to a change of the trend in the mean crust velocity of the upper km, from a landward increasing velocity to an almost constant one (Fig. 8).We speculate that the L2 bound could correspond to a transition from the fractured and eroded continental crust to the continental framework, which has acted as a second back-stop that has favored the formation of the basin (Wang and Hu, 2006; Byrne et al., 1993), although deeper velocity information is needed to confirm this. L2 also coincides with the fault zone 3, which is responsible of a 1.5 km offset in the continental basement, and controls the position of the Iquique Basin depocenter (Figs. 5 and 7). The prominent displacement in this fault zone needs that these faults penetrate several kilometers into the continental crust, and the dip of these faults in depth is probably similar to the dip (~70°) of intraplate seismicity (Ruiz et al., 2019) such as the March 16 foreshock focal mechanism.

Comparing four models for the Iquique earthquake slip distribution (Fig. 10), all show a similar peak slip location and width of the high slip zone, for example, if we define "high slip" by where the slip is greater than half of the peak slip. One can see that the limits of the Iquique Basin are correlated (using the spatially correlation defined previously) with the region of high slip (Fig. 9). This is in agreement with the idea that the inner wedge, where the basin lies, corresponds to the velocity weakening zone of the wedge (Wang and Hu, 2006), and that the coseismic extensional stresses (Geersen et al., 2018), enhanced by basal erosion (Noda, 2016), are forming the Iquique Basin. Also, the region that slipped during the main shock experienced a slow slip event with displacement of 150 cm on March 10–31, 2020 (Ruiz et al., 2014) and a diminution of the earth gravity field (Álvarez et al., 2015; Álvarez et al., 2018). A correlation between forearc basins and slip during large subduction earthquakes has been noted by other authors in subduction zones around the world (e.g. Fuller et al., 2006, Wells et al., 2003, Song and Simons, 2003, and by Álvarez et al., 2014, Álvarez et al., 2019). On the other hand, Noda (2016) suggested that earthquake slip and the velocity weakening zone are related to subsidence in the continental basement and basin formation in non-accretionary margins.

Finally, the slab obtained here with seismic data has a smaller angle of subduction and is shallower than both slab 1.0 and slab 2.0 (Hayes et al., 2012), at least in the first kilometers in the Iquique area. This should have a great impact on predicted slip distribution of the inversion models. In order to predict a better slip distribution near the trench in general, we should consider a slab model constrained not only by seismic activity (as slab 1.0 and slab 2.0), but also by shallow constrains as seismic reflection profiles and seismic velocity tomographies. In this particular earthquake is probably not very important as the predicted slip occurs in the deeper part of the contact, where the slab is better constrained due to GPS station distribution.

## 6. Conclusions

There is an important relation between the velocity structure of the continental wedge, the geologic structures and the seismic activity on the plate boundary. The outer wedge (first 20 km) is formed by a ~ 10-km wide frontal prism (between the trench and limit P) and ~ 10-km wide zone of a highly fractured continental crust (between limit P and limit ZF). During the 2010 $M_w$ 8.1 seismic sequence, the coseismic slip did not reach this low velocity zone and no aftershocks occurred. Consequently, this zone is interpreted to be a velocity strengthening zone of the plate boundary, although one cannot out rule the possibility that lack of aftershocks in the frontal zone can be due to localization problems. This zone is characterized by evidence for compressional deformation with limited evidence for normal faulting. In contrast the inner wedge (middle and upper slope) shows extensive normal faulting, with some important faults possibly penetrating deep into the continental crust. Particularly, the large intra plate seismicity with focal mechanisms coinciding with the faults seen in the continental basement as well as the large deformation seen in the Iquique Basin (fault zone 3) suggest the existence of large normal faults penetrating deep into the crust.

The region between km 55 and km 85 of the MC06 profile, may represent a 30 km wide transition zone without high coseismic slip but with great aftershock presence. The next 50 km (km 85–125; Fz2 and Fz3), corresponds to the region of high coseismic slip on the plate boundary and is correlated with the presence of the Iquique Basin, suggesting long term extensional deformation due to coseismic extensional stresses, as proposed by Geersen et al., 2018, and enhanced by basal subduction erosion. The Iquique Basin exhibits a landward migration of its depocenter, with older sediments forming a paleo-basin on the trench-ward side of it and younger sediments concentrated mainly in the landward side of the basin. This suggests landward migration of the trench and seismogenic zone through time and erosion (both from above and below) of the outer wedge. Growth strata and harpoon structures in the younger sediments suggest that the active normal structures are located mainly in the landward half of the basin. From the presence of harpoon structures we can also conclude that this portion of the wedge has not only been affected by normal stresses due to basal erosion and coseismic extension, but also compressional stresses, probably related to interseismic compression, in agreement with the March 16th reverse-faulting foreshock.

## Declaration of Competing Interest

The authors declare that they have no known competing financial interests or personal relationships that could have appeared to influence the work reported in this paper.

## Acknowledgments

We acknowledge the support of Programa de Investigación Asociativa (PIA): ANILLOS DE INVESTIGACION EN CIENCIA Y TECNOLOGÍA, CONICYT, grant ACT172002. We also thank the support and funding of CONICYT through the FONDECYT grant 1170009.

Cruise MGL1610 of the R/V *Marcus Langseth* was supported by the U. S. National Science Foundation under grant OCE-1459368. MCS data are available from the MGDS Academic Seismic Portal at Lamont-Doherty Earth Observatory (http://www.marine-geo.org/collections/#!/collection/Seismic#summary). All other cruise data are available through www.rvdata.org. We also acknowledge the contribution of the whole PICTURES working group for making this paper possible.

## Appendix A. Appendix 1

Using permanent displacement of GPS stations from the CSN (Centro Sismológico Nacional) a slip inversion is performed to confirm slip models found in previous papers. The inversion uses the Okada Model for calculating the displacement and the Slab 1.0 model (Hayes et al., 2012) for the subduction surface. It also uses a correlation length $\lambda = 10$ (smoothing parameter) and constrains the rake angle of each cell to +/− 5° of the main rake. We see a slip distribution similar (Fig. 10) to previous models (Ruiz et al., 2014), Schurr et al. (2014), Duputel et al. (2015)) characterized by a main patch at around 100 km in the N-S direction, between 19.3°S and 20.3°S with a maximum slip of approximately 6 m.

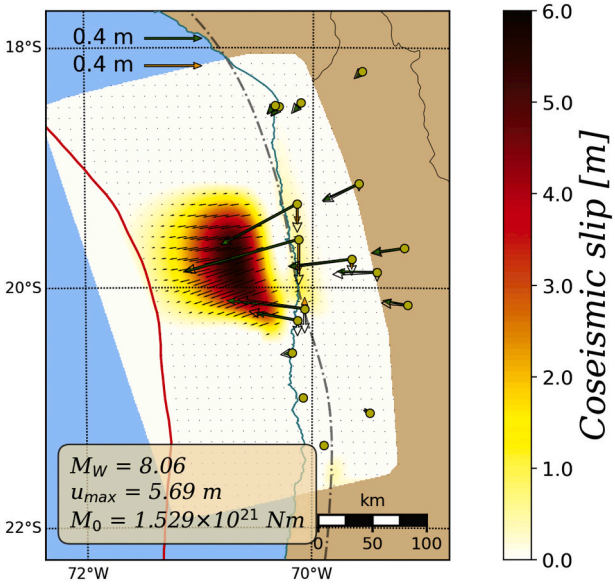


**Fig. A1.** Coseismic slip of the Iquique earthquake using permanent displacement of GPS stations of CSN. White arrows correspond to actual displacement, colored arrows correspond to predicted displacement with the slip model.

## References


Álvarez, O., Nacif, S., Gimenez, M., Folguera, A., Braitenberg, C., 2014. GOCE derived vertical gravity gradient delineates great earthquake rupture zones along the Chilean margin. Tectonophysics 622, 198–215. https://doi.org/10.1016/j.tecto.2014.03.011.

Álvarez, O., Nacif, S., Spagnotto, S., Folguera, A., Gimenez, M., Chlieh, M., Braitenberg, C., 2015. Gradients from GOCE reveal gravity changes before Pisagua Mw = 8.2 and Iquique Mw = 7.7 large megathrust earthquakes. J. S. Am. Earth Sci. 64, 273–287. https://doi.org/10.1016/j.jsames.2015.09.014.

Álvarez, O., Gimenez, M., Folguera, A., Guillen.,S (2018). Goce derived geoid changes before the Pisagua 2014 earthquake. Geod. Geodyn. doi:https://doi.org/10.1016/j.geog.2017.09.005.

Álvarez, O., Gimenez, M., Folguera, A., Chaves, C.A.M., Braitenberg, C., 2019. Reviewing megathrust slip behavior for recent Mw>8.0 earthquakes along the Peru-Chilean margin from satellite GOCE gravity field derivatives. Tectonophysics 769, 228188. https://doi.org/10.1016/j.tecto.2019.228188.

Armijo, R., Thiele, R., 1990. Active faulting in northern Chile: ramp stacking and lateral decoupling along a subduction plate boundary? Earth Planet. Sci. Lett. 98 (1), 40–61.

Bahlburg, H., Vervoort, J.D., Du Frane, S.A., Bock, B., Augustsson, C., Reimann, C., 2009. Timing of crust formation and recycling in accretionary orogens: insights learned from the western margin of South America. Earth Sci. Rev. 97 (1–4), 215–241.

Bassett, D., Watts, A.B., 2015. Gravity anomalies, crustal structure, and seismicity at subduction zones: 2. Interrelationships between fore-arc structure and seismogenic behavior. Geochem. Geophys. Geosyst. 16, 1541–1576. https://doi.org/10.1002/2014GC005685.

Bassett, D., Sandwell, D.T., Fialko, Y., Watts, A.B., 2016. Upper-plate controls on co-seismic slip in the 2011 Magnitude 9.0 Tohoku-oki earthquake. Nature. https://doi.org/10.1038/nature16945.

Becerra, J., Contreras-Reyes, E., Arriagada, C., 2013. Seismic structure and tectonics of the southern Arauco Basin, south-Central Chile (~ 38 S). Tectonophysics 592, 53–66.

Becerra, J., Arriagada, C., Contreras-Reyes, E., Bascuñan, S., De Pascale, G.P., Reichert, C., Díaz-Naveas, J., Cornejo, N., 2017. Gravitational deformation and inherited structural control on slope morphology in the subduction zone of north-Central Chile (ca. 29–33° S). Basin Res. 29 (6), 798–815.

Buchelt, M.; Tellez, C. 1988. The Jurassic La Negra Formation in the area of Antofagasta, northern Chile (lithology, petrography, geochemistry). In The Southern Central Andes (Bahlburg, H.; Breitkreuz; C.; Giese, P.; editors). Springer, Heidelberg. Lect. Notes Earth Sci. 17: 171–182.

Byrne, D.E., Wang, W., Davis, D.M., 1993. Mechanical role of backstops in the growth of forearcs. Tectonics 12 (1), 123–144.

Carrizo, D., González, G., Dunai, T., 2008. Constricción neógena en la Cordillera de la Costa, norte de Chile: Neotectónica y datación de superficies con 21Ne cosmogénico. Rev. Geol. Chile 35 (1), 1–38.

Charrier, R., Hérail, G., Pinto, L., García, M., Riquelme, R., Farías, M., Muñoz, N., 2013. Cenozoic tectonic evolution in the Central Andes in northern Chile and west Central Bolivia: implications for paleogeographic, magmatic and mountain building evolution. Int. J. Earth Sci. 102 (1), 235–264.

Comte, D., Pardo, M., 1991. Reappraisal of great historical earthquakes in the northern Chile and southern Peru seismic gaps. Nat. Hazards 4 (1), 23–44. https://doi.org/10.1007/bf00126557.

Contardo, X., Cembrano, J., Jensen, A., Díaz-Naveas, J., 2008. Tectono-sedimentary evolution of marine slope basins in the Chilean forearc (33 30′–36 50′ S): insights into their link with the subduction process. Tectonophysics 459 (1–4), 206–218.

Contreras-Reyes, E., 2018. Structure and tectonics of the chilean convergent margin from wide-angle seismic studies: a review. In: Folguera, A., et al. (Eds.), The Evolution of the Chilean-Argentinean Andes. Springer Earth System Sciences. Springer, Cham, pp. 3–29. https://doi.org/10.1007/978-3-319-67774-3_1.

Contreras-Reyes, E., Jara, J., Grevemeyer, I., Ruiz, S., Carrizo, D., 2012. Abrupt change in the dip of the subducting plate beneath North Chile. Nat. Geosci. 5 (5), 342.

Contreras-Reyes, E., Ruiz, J.A., Becerra, J., Kopp, H., Reichert, C., Maksymowicz, A., Arriagada, C., 2015. Structure and tectonics of the central Chilean margin (31°-33° S): Implications for subduction erosion and shallow crustal seismicity. Geophys. J. Int. 203 (2), 776–791.

Cosentino, N.J., Jordan, T.E., 2017. $^{87}Sr/^{86}Sr$ of calcium sulfate in ancient soils of hyperarid settings as a paleoaltitude proxy: Pliocene to Quaternary constraints for northern Chile (19.5–21.7°S). Tectonics 36, 137–162. https://doi.org/10.1002/2016TC004185.

Delouis, B., Philip, H., Dorbath, L., Cisternas, A., 1998. Recent crustal deformation in the Antofagasta region (northern Chile) and the subduction process. Geophys. J. Int. 132 (2), 302–338.

DeMets, C., Gordon, R.G., Argus, D.F., 2010. Geologically current plate motions. Geophys. J. Int. 181 (1), 1–80.

Dunai, T.J., Gonzalez-Lopez, G.A., Juez-Larre, J., Carrizo, D., 2005. Preservation of (early) miocence landscapes in the Atacama Desert, northern Chile. Geochim. Cosmochim. Acta 69 (10), A161.

Duputel, Z., et al., 2015. The Iquique earthquake sequence of April 2014: Bayesian modeling accounting for prediction uncertainty. Geophys. Res. Lett. 42 (19), 7949–7957.

Evenstar, L.A., Hartley, A.J., Stuart, F.M., Mather, A.E., Rice, C.M., Chong, G., 2009. Multiphase development of the Atacama Planation Surface recorded by cosmogenic 3He exposure ages: Implications for uplift and Cenozoic climate change in western South America. Geology 37, 27–30.

Evenstar, L.A., Mather, A.E., Hartley, A.J., Stuart, F.M., Sparks, R.S.J., Cooper, F.J., 2017. Geomorphology on geologic timescales: Evolution of the late Cenozoic Pacific paleosurface in Northern Chile and Southern Peru. Earth Sci. Rev. 171, 1–27.

Farías, M., Comte, D., Roecker, S., Carrizo, D., Pardo, M., 2011. Crustal extensional faulting triggered by the 2010 Chilean earthquake: the Pichilemu Seismic Sequence. Tectonics 30 (6).

Fuller, C.W., Willett, S.D., Brandon, M.T., 2006. Formation of forearc basins and their influence on subduction zone earthquakes. Geology 34 (2), 65–68.

Geersen, J., Ranero, C.R., Kopp, H., Behrmann, J.H., Lange, D., Klaucke, I., Barrientos, S., Diaz-Naveas, J., Barckhausen, U., Reichert, C., 2018. Does permanent extensional deformation in lower forearc slopes indicate shallow plate-boundary rupture? Earth Planet. Sci. Lett. 489, 17–27.

Hartley, A.J., May, G., Chong, G., Turner, P., Kape, S.J., Jolley, E.J., 2000. Development of a continental forearc: a Cenozoic example from the Central Andes, northern Chile. Geology 28 (4), 331–334.

Hayes, G.P., Wald, D.J., Johnson, R.L., 2012. Slab1. 0: a three-dimensional model of global subduction zone geometries, Journal of Geophysical Research: Solid Earth, 117(B1).Kato, a., and S. Nakagawa (2014), Multiple slow-slip events during a foreshock sequence of the 2014 Iquique, Chile Mw 8.1 earthquake. Geophys. Res. Lett. 41 (15), 5420–5427.

Kato, A., Nakagawa, S., 2014. Multiple slow-slip events during a foreshock sequence of the 2014 Iquique, Chile Mw 8.1 earthquake. Geophys. Res. Lett. 41 (15), 5420–5427.
Lay, T., Yue, H., Brodsky, E.E., An, C., 2014. The 1 April 2014 Iquique, Chile, Mw 8.1 earthquake rupture sequence. Geophys. Res. Lett. 41 (11), 3818–3825.
León-Ríos, S., Ruiz, S., Maksymowicz, A., Leyton, F., Fuenzalida, A., Madariaga, R., 2016. Diversity of the 2014 Iquique's foreshocks and aftershocks: clues about the complex rupture process of a Mw 8.1 earthquake. J. Seismol. 20 (4), 1059–1073.
Li, D., Liu, Y., 2017. Modeling slow-slip segmentation in Cascadia subduction zone constrained by tremor locations and gravity anomalies. J. Geophys. Res. Solid Earth 122 (4), 3138–3157.
Loewy, S.L., Connelly, J.N., Dalziel, I.W., 2004. An orphaned basement block: the Arequipa-Antofalla Basement of the central Andean margin of South America. Geol. Soc. Am. Bull. 116 (1–2), 171–187.
Maksymowicz, A., Ruiz, J., Vera, E., Contreras-Reyes, E., Ruiz, S., Arraigada, C., Bonvalot, S., Bascuñán, S., 2018. Heterogeneous structure of the Northern Chile marine forearc and its implications for megathrust earthquakes. Geophys. J. Int. 215 (2), 1080–1097.
Mamani, M., Wörner, G., Sempere, T., 2010. Geochemical variations in igneous rocks of the Central Andean orocline (13°S to 18°S): Tracing crustal thickening and magma generation through time and space. Geol. Soc. Am. Bull. 2010 122 (1–2), 162–182.
Melnick, D., 2016. Rise of the central Andean coast by earthquakes straddling the Moho. Nat. Geosci. 9 (5), 401.
Noda, A., 2016. Forearc basins: types, geometries, and relationships to subduction zone dynamics. Bulletin 128 (5–6), 879–895.
Oliveros, V., Morata, D., Aguirre, L., Féraud, G., Fornari, M., 2007. Jurassic to early cretaceous subduction-related magmatism in the Coastal Cordillera of northern Chile (18°30′-24°S): geochemistry and petrogenesis. Rev. Geol. Chile 34 (2), 209–232.
Oliveros, V., Vásquez, P., Creixell, C., Lucassen, F., Ducea, M.N., Ciocca, I., González, J., Espinoza, M., Salazar, E., Coloma, F., Kasemann, S.A., 2020. Lithospheric evolution of the Pre-and early Andean convergent margin, Chile. Gondwana Res. 80, 202–227.
Ranero, C.R., von Huene, R., Weinrebe, W., Reichert, C., 2006. Tectonic Processes Along the Chile Convergent Margin, in the Andes. Springer, pp. 91–121.
Ruiz, J.A., Maksymowicz, A., Ortega-Culaciati, F., Rivera, L., Comte, D., 2019. Source characteristics of the March 16, 2014 Mw 6.7 earthquake and its implications for the Mw 8.2 Pisagua mainshock. Tectonophysics 767, 228170.
Ruiz, S., Metois, M., Fuenzalida, A., Ruiz, J., Leyton, F., Grandin, R., Vigny, C., Madariaga, R., Campos, J., 2014. Intense foreshocks and a slow slip event preceded the 2014 Iquique Mw 8.1 earthquake. Science 345 (6201), 1165–1169.
Rutland, R., 1971. Andean orogeny and ocean floor spreading. Nature 233 (5317), 252.
Sallares, V., Ranero, C., 2005. Structure and tectonics of the erosional convergent margin off Antofagasta, North Chile (23 degrees 30'S)-art. No. B06101. J. Geophys. Res. Solid Earth 110 (B6). NIL.
Schellart, W.P., 2017. Andean mountain building and magmatic arc migration driven by subduction-induced whole mantle flow. Nat. Commun. 8, 2010. https://doi.org/10.1038/s41467-017-01847-z.
Schurr, B., et al., 2014. Gradual unlocking of plate boundary controlled initiation of the 2014 Iquique earthquake. Nature 512 (7514), 299.
Sempere, T., Carlier, G., Soler, P., Fornary, M., Carlotto, V., Jacay, J., Arispe, O., Nereudeau, 584 D., Cárdenas, J., Rosas S. and Jiménez, N., 2002. Late Permian-Middle Jurassic lithospheric thinning in Peru and Bolivia, and its bearing on Andean-age tectonics. Tectonophysics 345 (1–4), 153–181.
SERNAGEOMIN, 2003. Mapa Geológico de Chile: versión digital. Servicio Nacional de Geología y Minería, Publicación Geológica Digital, No. 4 (CD-ROM, versión1.0, 2003) (Santiago).
Song, T.-R.A., Simons, M., 2003. Large trench-parallel gravity variations predict seismogenic behavior in subduction zones. Science 301 (5633), 630–633.
Soto, H., Sippl, C., Schurr, B., Kummerow, J., Asch, G., Tilmann, F., Comte, D., Ruiz, S., Oncken, O., 2019. Probing the Northern Chile Megathrust with Seismicity: the 2014 M8. 1 Iquique Earthquake Sequence. J. Geophys. Res. Solid Earth 124 (12), 12935–12954.
Spagnotto, S., Alvarez, O., Folguera, A., 2018. Static Stress Increase in the Outer Forearc Produced by M W 8.2 September 8, 2017 Mexico Earthquake and its Relation to the Gravity Signal. Pure Appl. Geophys. 175 (8), 2575–2593.
Tréhu, A.M., de Moor, A., Madrid, J.M., Sáez, M., Chadwell, C.D., Ortega-Culaciati, F., Ruiz, J., Ruiz, S., Tryon, M.D., 2020. Post-seismic response of the outer accretionary prism after the 2010 Maule earthquake, Chile. Geosphere 16 (1), 13–32.
Von Huene, R., Ranero, C.R., 2003. Subduction erosion and basal friction along the sediment-starved convergent margin off Antofagasta, Chile. J. Geophys. Res. Solid Earth 108 (B2).
Von Huene, R., Kulm, L., Miller, J., 1985. Structure of the frontal part of the Andean convergent margin. J. Geophys. Res. Solid Earth 90 (B7), 5429–5442.
Von Huene, R., Weinrebe, W., Heeren, F., 1999. Subduction erosion along the North Chile margin. J. Geodyn. 27 (3), 345–358.
Wang, K., Hu, Y., 2006. Accretionary prisms in subduction earthquake cycles: the theory of dynamic Coulomb wedge. J. Geophys. Res. Solid Earth 111 (B6). https://doi.org/10.1029/2005jb004094.
Wells, R.E., Blakely, R.J., Sugiyama, Y., Scholl, D.W., Dinterman, P.A., 2003. Basin-centered asperities in great subduction zone earthquakes: a link between slip, subsidence, and subduction erosion? J. Geophys. Res. Solid Earth 108 (B10).
Wörner, G., Uhlig, D., Kohler, I., Seyfried, H., 2002. Evolution of the West Andean Escarpment at 18°S (N. Chile) during the last 25 Ma: uplift, erosion and collapse through time. Tectonophysics 345 (1–4), 183–198.